# Asymmetric influence of the amplitude-dependent tune shift on the transverse mode-coupling instability

Miriam Brosi,* Francis Cullinan, Åke Andersson, Jonas Breunlin, and Pedro Fernandes Tavares
*MAX IV Laboratory, Lund University, Lund, Sweden*

(Received 18 April 2024; accepted 30 September 2024; published 25 October 2024)

At the 3 GeV ring of the MAX IV Laboratory, a fourth-generation ring-based synchrotron light source, an asymmetric influence of the sign of the amplitude-dependent tune shift (ADTS) on the transverse mode-coupling instability has been observed. Measurements of the instability, in dedicated single-bunch experiments at low chromaticity, revealed a significant dependence of the dynamics of the instability above threshold on the sign of the ADTS. While for a negative sign of the ADTS, the crossing of the instability does not lead to a loss of beam current, a positive sign results in the loss of 40% or more of the beam current at the threshold. In order to investigate the observed asymmetry, the systematic measurement of beam dynamics above the threshold has been conducted in combination with particle tracking simulations with MBTRACK2 and theoretical calculations of the Landau damping due to the ADTS. The findings point toward an influence of the Landau damping in combination with the low synchrotron frequency, which indicates that this effect could become relevant in the future low-emittance electron storage rings.

DOI: 10.1103/PhysRevAccelBeams.27.104402

## I. INTRODUCTION

The transverse mode-coupling instability (TMCI) in electron storage rings is a single-bunch transverse instability and an important collective effect, which can limit the parameter space for stable operation. Especially in fourth-generation light sources, this collective effect can strongly influence the achievable operation parameters. The instability depends on many beam parameters like the natural bunch length, the chromaticity, and the tunes. The connection with the amplitude-dependent tune shift (ADTS) was in the past investigated in the interest of mitigation of transverse instabilities by Landau damping [1–3], as the required betatron tune spread can among other sources come from the ADTS.

The first studies of the influence of the ADTS on the TMCI for the 3 GeV ring at the MAX IV Laboratory where presented by several of the authors in [4–6]. While in the case of MAX IV, the TMCI does not affect routine operation, it is nevertheless important to characterize and further investigate such instabilities as with the continuous push toward more extreme operation modes and beam parameters new effects and interaction between parameters can arise and become relevant for the mitigation of such instabilities in future machines.

Dedicated, systematic experiments have now been conducted in a single-bunch operation showing an asymmetric influence of the sign of the ADTS on the dynamics of the vertical TMCI above threshold. While the ADTS does not significantly affect the threshold current, it changes the behavior of the bunch above threshold. For values of the ADTS close to zero, a partial beam loss is observed when the threshold current is crossed while slowly increasing the bunch current. For ADTS with a large absolute value, on the other hand, the beam loss is not observed as the threshold is crossed, and the instability leads solely to oscillations of the bunch center of mass and a beam size blowup. For a positive sign of the ADTS, this partial beam loss occurs up to higher values of the ADTS than for a negative sign, resulting in a significant asymmetry in the encountered beam loss above threshold.

An asymmetric influence of the sign of the ADTS coefficient on the threshold currents of head-tail instabilities is well known and exploited at hadron machines, e.g., LHC [7–9] and FCC-hh [10]. A similar asymmetry was also observed during the study of coupled-bunch instabilities at the ELETTRA electron storage ring [11]. The impact of the ADTS on the TMCI, on the other hand, is less clear since, as pointed out by Métral [12], for Landau damping to play a role, the tune spread within a bunch needs to be in the order of the synchrotron tune. Landau

*Contact author: miriam.brosi@maxiv.lu.se

damping has even been predicted to reduce the threshold current of the TMCI in specific cases [12,13]. However, typically, no great dependence of the threshold is observed, e.g., [14], and that is also the case here. It is perhaps for this reason that this topic has not been studied previously in as much depth.

In the present study, the beam dynamics above the TMCI threshold can be investigated at ADTS values where no beam loss occurs. This is used to investigate the observed asymmetry further. It is observed that, as expected, the instability leads to a blowup of the bunch size and strong center-of-mass oscillations. For negative ADTS values and at high current at high positive ADTS values, these oscillations are additionally amplitude-modulated with a much lower frequency showing a sawtooth shaped pattern.

This paper compares the measurements conducted at the MAX IV Laboratory with dedicated simulations and theoretical considerations. The measurements include systematic scans of the instability threshold and the occurring current loss as well as time-resolved measurements of the beam dynamics, in this case, the center-of-mass motion and the transverse bunch size, above the threshold current. The simulations consist of particle tracking with the MBTRACK2 code [15], which allows the inclusion of the amplitude-dependent tune shift. The theoretical calculation considering transverse mode coupling and Landau damping due to the ADTS was conducted as described in the next section and Sec. IV D.

### A. Transverse mode-coupling instability

The transverse mode-coupling instability can arise when the current-dependent tune shift due to the transverse impedance leads to a coupling of the coherent betatron tune with one of the neighboring head-tail mode frequencies (typically the mode $-1$ with a separation of $-\nu_s$, the synchrotron tune). The TMCI, which occurs at zero chromaticity, has, opposed to the head-tail instability, a well-defined threshold current at which the growth rate increases abruptly. Figure 1 shows the simulated mode coupling at zero chromaticity.

The theory of Landau damping in combination with transverse mode coupling has been developed by Chin [13] for the case of no coherent perturbations. It is characterized by a dispersion integral written as

$$I_m = -2\pi \int_0^\infty \frac{J}{V - m\nu_s - \nu_\beta - \Delta\nu(J)} \left(\frac{df}{dJ}\right) dJ, \quad (1)$$

where $V$ is the complex coherent tune of the instability to be found, $J$ is the action of betatron oscillation, $\nu_\beta$ and $\nu_s$ are the betatron and synchrotron tunes, respectively, $f$ is the normalized charge distribution in $J$ of the bunch and $\Delta\nu(J)$ is the amplitude-dependent tune shift (ADTS) giving rise to the tune spread between the individual electrons within the bunch.

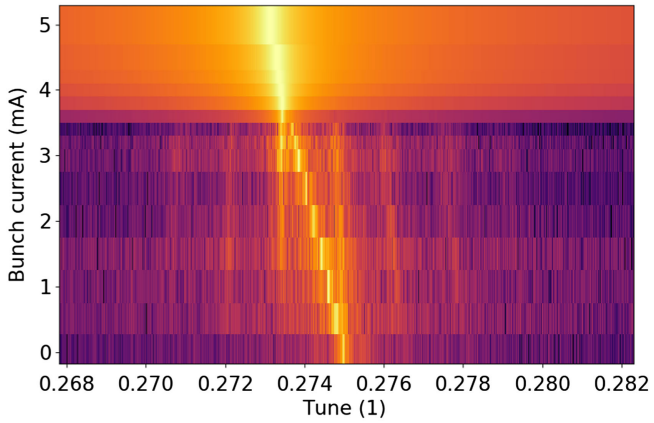


FIG. 1. Simulated coherent beam spectrum of the bunch at zero chromaticity and zero ADTS, showing the tune shift with increasing bunch current and the resulting mode coupling at the TMCI threshold at 3.5 mA.

For the theoretical calculations, a simplified model with a Gaussian charge distribution is assumed:

$$f(J) = \frac{1}{2\pi\langle J\rangle} e^{-\frac{J}{\langle J\rangle}}, \quad (2)$$

where $\langle J\rangle$ is the average action of the particle ensemble. For our purposes, the tune shift is assumed to be proportional to the action $J$ resulting in the following definition for a single particle where $b$ is the amplitude-dependent tune shift coefficient:

$$\Delta\nu(J) = b\,J. \quad (3)$$

In the following, when a value for the ADTS coefficient is given, it refers to $b$ and has the unit $[b] = 1/\mathrm{m}$, if not stated otherwise.

Evaluating the integral in Eq. (1) gives

$$I_m = -\frac{1}{b\langle J\rangle}[1 + \zeta e^{-\zeta} E_1(-\zeta)], \quad \text{where } \zeta > 0 \quad (4)$$

and

$$\zeta = \frac{V - \nu_\beta - m\nu_s}{b\langle J\rangle}. \quad (5)$$

Solutions with small and positive growth rates $\mathrm{Im}(V) > 0$ lie on the boundary of stability. To include radiation damping, we could set $\mathrm{Im}(V) = +1/\tau_x$, where $\tau_x$ is the radiation damping time. Here, however, we neglect radiation damping as it does not make a large difference in the case of the TMCI. An added benefit is that Eq. (4) is then scalable by $b$ and so only needs to be evaluated twice, once for $b > 0$ and once for $b < 0$.

The inverse of the dispersion relation is subtracted from the diagonal elements of Chin's scaled coupling matrix $\nu_s \mathbf{M}_{nl}^{mk}$ for head-tail and mode-coupling instabilities as given by Eq. 2.44 in [13]. Solutions are determined numerically by equating the determinant of the resulting matrix to zero:

$$\det(I_m^{-1}\delta_{ml}\delta_{nk} - \nu_s \mathbf{M}_{nl}^{mk}) = 0, \tag{6}$$

where $\delta_{ij}$ is the Kronecker delta. In practice, there are two unknowns left to determine: the tune spread at $\langle J \rangle$ (for a Gaussian distribution, the tune spread is equal to the tune shift of a particle at the position of $\langle J \rangle$: $\sigma_\nu = b\langle J \rangle = \Delta\nu(\langle J \rangle)$, see Appendix B) and the coherent frequency of oscillation $\mathrm{Re}(V)$.

## II. EXPERIMENTAL SETUP

The measurements presented in this paper were performed with the machine parameters given in Table I if not stated otherwise. Only a single bunch was stored in the machine to be able to use diagnostics that are not bunch-resolved, such as beam position monitors (BPM) and the synchrotron light monitor (SLM). To ensure that only a pure single bunch is filled, great care has been taken to clean out residual charge from the other buckets. The used BPMs and the used SLM sit at different positions in the ring, and therefore, at different values of the beta function. To make the bunch sizes and center-of-mass positions shown within this publication comparable, all measurements are scaled to correspond to a measurement at a beta function of 16.0 m. This value was chosen as it is the beta function at the position of the used SLM and is very close to the maximal vertical beta function of 16.1 m. To translate the measured values to this position, they are scaled with the ratio of the square roots of the goal beta function value and the original value at the place of measurement.

The total acceleration voltage in the main cavities was set to a fixed value for better comparability of different measurements. Due to the usage of a single bunch, and therefore, a low absolute beam current, the passive Landau cavities are not elongating the bunch. Likewise, all insertion device gaps were opened for the sake of comparability. The reference orbit for the orbit correction was set to zero-orbit without any beamline bumps[1] laid in, to use an optic close to the design optics used in the simulations. During the measurements, the orbit correction was only in use while changing to new settings, e.g., changing chromaticity or ADTS, and was afterward switched off. When changing settings, it was also checked that the tunes were at the routine working point. The vertical chromaticity was reduced via sextupole magnets in the vertical plane while the horizontal chromaticity remained at the value for routine operation of around 1.1. For adjustments of the ADTS, three octupole magnet families are available [16].

TABLE I. Beam parameters during measurements.

| Parameter | Value |
|---|---|
| Beam energy (GeV) | 3.0 |
| Circumference (m) | 528 |
| RF frequency (MHz) | 99.931 |
| Harmonic number | 176 |
| RF voltage (kV) | 864 |
| Synchrotron frequency (Hz) | 830 |
| Synchrotron tune | 0.00146 |
| Vertical tune | 16.275 |
| Vertical beta function (m) | 2.0 to 16.1 |
| Horizontal tune | 42.2 |
| Horizontal beta function (m) | 0.8 to 9.8 |

### A. ADTS—Measurement and control

The center-of-mass (COM) motion is measured via the turn-by-turn data from the BPMs. The position at each turn can be written out for $2^{16}$ consecutive turns. As the measurements where taken in a single-bunch operation, this gives the COM position of the bunch at each turn at every BPM. The coherent tunes can, therefore, be calculated from the Fourier transform of this data.

The amplitude-dependent tune shift was measured by kicking the bunch in each transverse plane individually with increasing amplitude while detecting the center-of-mass movement on the turn-by-turn BPM data for both transverse planes. The tune was calculated via the Numerical Analysis of Fundamental Frequencies algorithm [17,18] based on the first 100 turns[2] after each kick. The resulting tunes for the different kick amplitudes show the tune shift as a function of the center-of-mass displacement $\hat{x}$ at each BPM position. For the conversion between the measured maximal amplitude $\hat{x}$ at each BPM and the action $J$, it is assumed that at maximum displacement $\hat{x}$ the action $J$ can be calculated via the corresponding value of the beta function $\beta_s$ at the position of measurement $s$, in this case the position of each BPM:

$$J = \frac{\hat{x}_s^2}{\beta_s}. \tag{7}$$

Figure 2 shows the near-linear dependence of the tune shift on the action $J$ in an example measurement.

To ease the operation during the experimental scans of the ADTS value, a response matrix $M$ was measured for the resulting change of the ADTS caused by changes to two of

[1]Beamline bumps refer to deliberate deviations in the closed orbit at the position of IDs to help synchrotron radiation alignment for beamlines.

[2]The number of 100 turns was chosen to provide a sufficient resolution for the calculated shift in tune while staying below the turn number above which decoherence sets in.

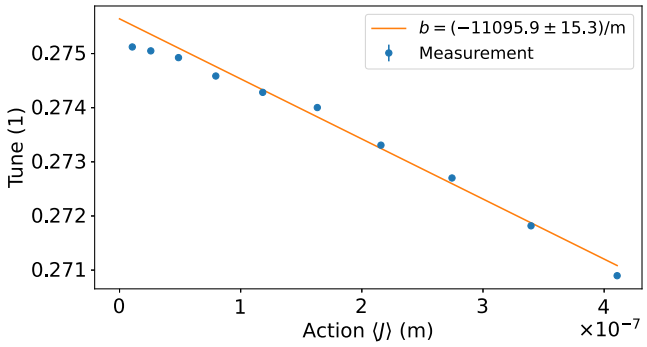


FIG. 2. Measurement of the betatron tune as a function of the action $\langle J \rangle$ in the vertical plane, showing the linear dependence giving the amplitude-dependent tune shift coefficient $b$.

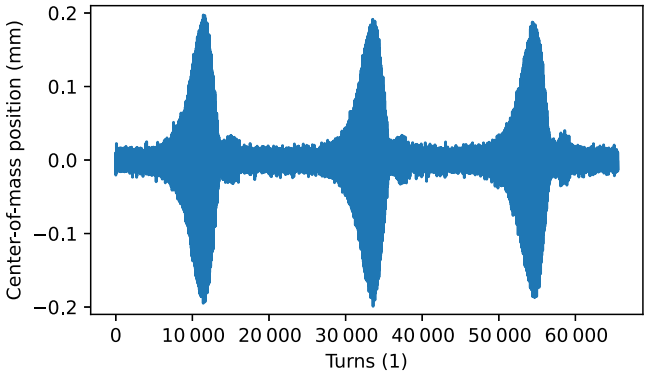


FIG. 3. BPM signal showing the amplitude modulation caused by the TMCI on the vertical center-of-mass position as a function of turns for an ADTS coefficient of $b = -6868/\mathrm{m}$ and 4.5 mA.

the octupole families. This matrix allows fast calculation of the necessary change $\Delta I_{\mathrm{oct,u}}$ in octupole magnet current for a requested change of $\Delta b_{\mathrm{u}}$ in ADTS coefficient, with $u$ representing the planes $x$ and $y$, without the need for intermediate measurements:

$$\begin{pmatrix} \Delta I_{\mathrm{oct,x}} \\ \Delta I_{\mathrm{oct,y}} \end{pmatrix} = M^{-1} * \begin{pmatrix} \Delta b_{\mathrm{x}} \\ \Delta b_{\mathrm{y}} \end{pmatrix}. \tag{8}$$

Nevertheless, after arriving at a new ADTS value and checking, and if necessary correcting, the chromaticity and the tunes, and before conducting dedicated measurements, the ADTS value was measured to ensure accuracy.

### B. Transverse bunch size

The transverse bunch size is measured at the two diagnostic beamlines [19] via synchrotron light monitors (SLM) with interferometric source point imaging. Synchrotron radiation in the visible wavelength range is detected with CMOS cameras after passing though a double-slit for the horizontal plane and a diffraction obstacle in the vertical plane. The beam sizes can be calculated from the interferometric visibility in the resulting interference pattern [19]. During the instability, the bunch size is blown up to such a degree that the interference pattern is not visible anymore [Fig. 4(b)] and the distribution is fitted by a Gaussian. The required exposure time of the cameras to gather enough intensity does not allow for turn-by-turn detection. Nevertheless, the exposure time is short enough ($\approx$1 ms) to allow resolving the time structure of the characteristic amplitude modulation observed on the center-of-mass position (see Fig. 3) caused by the dynamics above the instability threshold. In this case, it has to be taken into account that during the exposure time, the camera integrates over the observed center-of-mass oscillations providing a superposition of the center-of-mass motion and the interference pattern containing the beam size information. Furthermore, it has to be asserted that no residual bunches are present during these measurements.

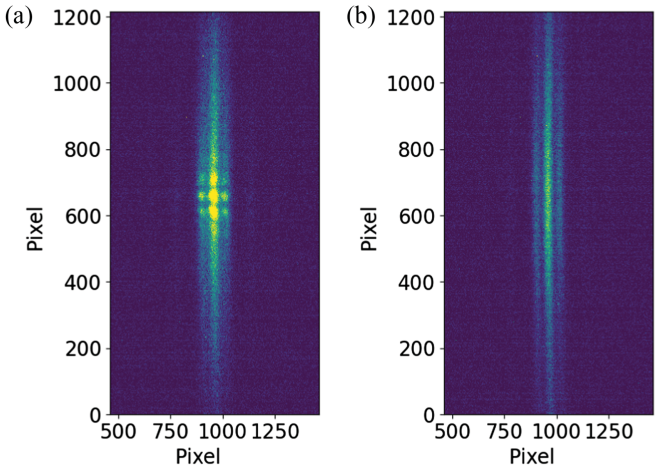


FIG. 4. Synchrotron light spot of a vertically unstable bunch measured at a diagnostic beamline for interferometric bunch size measurement. (a) The additional, residual low-current bunches are stable and show the typical interferometric pattern on top of the unstable main bunch. (b) After cleaning the residual bunches, only the vertically unstable single bunch is visible.

As visible in Fig. 4, even a small amount of charge in additional residual bunches around the main single bunch, in this case approximately 5% of the charge, can significantly influence the observed spot profile on the SLMs. As these low-charge residual bunches are below the instability threshold and therefore stable, their light shows the classical interference pattern. The intensity of the focused pattern is, therefore, overshadowing the smeared-out spot profile from the unstable main bunch.

### C. Synchronized measurements

The acquisition by the cameras can be triggered so that synchronized images can be taken relative to the turn-by-turn center-of-mass motion measured with the BPMs. The synchronization was aligned with triggered kicks from a pulsed magnet to the beam that can be observed in both

systems (BPMs and SLMs). The timing between the camera acquisition and BPM acquisition is chosen such that the camera's exposure time window lies roughly at three-quarters of the BPM measurement window of $2^{16}$ turns (≈115 ms). By this, the center-of-mass movement is known for some time before and after the bunch size measurement. The alignment accuracy depends on the camera exposure time used and is in the presented measurements better than 1 ms.

In case of multiple such measurement sets being taken during the instability with the characteristic amplitude modulation on the center-of-mass movement (see Fig. 3), the repetitive behavior seen on the BPMs can be used to overlay multiple measurement sets aligned by this pattern. This will provide a "sampled" image of the changes in the light spot observed on the SLM cameras. In other words, due to the measurement trigger not being synchronized to the instability dynamics, different phases of the amplitude modulation are sampled with every measurement set taken and the repetitiveness of the amplitude modulation can be used to reconstruct a time resolved image. The spot size is the result of the superposition of the blown-up bunch size and the center-of-mass oscillation within the exposure time window.

## III. SIMULATION TOOL

To simulate the beam dynamics observed, especially above the threshold current, we performed particle tracking with the MBTRACK2 python code (tag 0.4) [15,20]. A python script to start the simulations, containing the used properties, is published in Supplemental Material [21].

A simple broadband resonator was used for the vertical impedance with a shunt impedance of 200 kOhm/m at the resonant frequency of 11.5 GHz and a quality $Q$ of 1 [22]. The MBTRACK2 simulations also included a longitudinal impedance (broadband resonator at 732 Ohm at 6 GHz with $Q = 1$ [4]) to account for bunch lengthening with increasing bunch current. MBTRACK2 allows for the optics parameter to be read-in from an AT lattice file using pyAT. The rf voltage was set to the same value as in the measurements (see Table I) and synchrotron radiation effects were included in the simulations. The tune shift contribution by the ADTS is calculated in MBTRACK2 based on the action $J$ [see Sec. I A Eq. (3)]. Intrabeam scattering (IBS) is not yet implemented in MBTRACK2. The simulations were conducted with 50 000 macro-particles and were run on the COSMOS cluster of LUNARC at Lund University. The center-of-mass amplitudes and bunch sizes are calculated in MBTRACK2 once per turn and for a value of the beta function of 7.23 m corresponding approximately to the average of the beta function along the ring. Therefore, all simulated COM amplitudes and bunch sizes were scaled to the same reference as the measurements, a beta function of 16.0 m.

## IV. RESULTS

In the following, the measurement and simulation results are presented side by side and grouped by the different beam properties affected by the instability. The measurements were conducted in the vertical plane. Besides the threshold current, the beam loss at threshold, the bunch position and size, as well as the betatron tune shift with current below and above the instability threshold are discussed. Additionally, theoretical calculations on the Landau damping in combination with the transverse mode-coupling instability will be discussed in the context of the observed asymmetry with respect to the sign of the amplitude-dependent tune shift.

### A. Instability threshold

When studying an instability, the threshold current is a very important parameter as it is the limit up to what current stable operation is possible.

We observed that the TMCI threshold current changes depending on the beam conditions while reaching the threshold. For example, the threshold current was lower when the beam current slowly decayed while the beam was unstable, compared to the threshold current when charge was injected into a stable beam. Additionally, within a certain bunch current range, it was possible to stabilize an unstable beam with the bunch-by-bunch feedback system and the beam remained stable after switching off the feedback. Furthermore, the instability could be triggered by excitations or kicks to the beam even below the injection threshold but not below the decaying threshold. In summary, we observed an hysteresis effect on the TMCI threshold current, where a stable beam shows a higher threshold current than an already unstable or excited beam.

A possible explanation for the threshold hysteresis is intrabeam scattering. For beams with small transverse emittances, IBS can lead, among other things, to an increase in energy spread. This can be mitigated by increasing the vertical emittance either via coupling or with vertical excitations of the beam. With respect to the TMCI, IBS would have the following effect. For a stable beam, the vertical emittance is small and the energy spread is increased by IBS. An increased energy spread results in an increase of the theoretical TMCI threshold, as the current-dependent tune shift is inversely proportional to the bunch length that again is proportional to the energy spread [23]. As soon as the beam becomes unstable, either by crossing the (higher) threshold or by excitation, the vertical emittance increases and the effect of the IBS is reduced leading to a reduction in energy spread. The lower energy spread finally results in a lower TMCI threshold current. This results in a hysteresis of the instability threshold depending on whether the threshold is measured starting with a stable or an unstable beam.

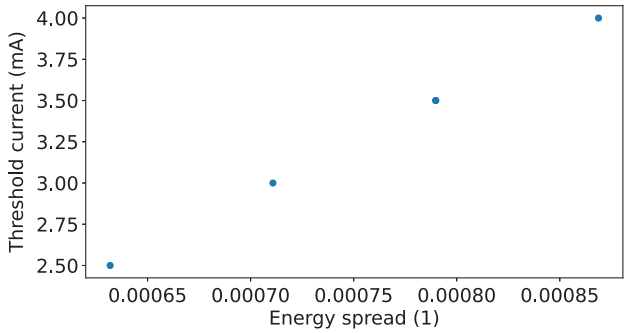


FIG. 5. Simulated TMCI threshold at a chromaticity of 0.05, $b = 1000$ and different energy spreads of 80%, 90%, 100%, and 110% showing the expected increase in threshold for increased energy spread.

As the MBTRACK2 simulations do not include IBS this hysteresis cannot be directly simulated. Nevertheless, simulations with the energy spread manually set to different values show the expected dependence of the threshold current on the energy spread (see Fig. 5).

For the following studies, the threshold during injection was selected as it can be quickly measured reliably and accurately compared to the other thresholds. Furthermore, the disturbance to the stored beam caused by the Multipole Injection Kicker (MIK) is known to be very small [24], so the observed threshold during injection should be very close to the theoretical threshold (including IBS) if the charge in a stable beam is slowly increased.

The left hand side of Fig. 6 shows the thresholds measured during injection for different ADTS coefficients. These thresholds were determined by injecting (using the MIK) into a single bunch and observing the center-of-mass movement on the BPMs. As soon as the center-of-mass movement grew unstable, the injection was stopped and all charge in residual bunches from a nonperfect single bunch injection was cleaned. The resulting threshold currents differ as expected depending on the chromaticity. To separate the TMCI from the head-tail instability [25], the measurements where conducted either at a vertical chromaticity $\xi_y$ of zero $(0.00 \pm 0.01)$ or nearly zero chromaticity $(0.05 \pm 0.02)$ in contrast to a chromaticity of $\approx 1.1$ during routine operation. The thresholds at both low chromaticity values ($\xi_y = 0.00$ and $\xi_y = 0.05$) are very similar and lie around 2.8 mA. Additionally, measurements were conducted at a slightly negative vertical chromaticity of $-0.15 \pm 0.10$. As expected during operation with a positive momentum compaction factor and a negative chromaticity (e.g. [23]), they show a much lower threshold current of around 1 mA. The same is visible in the simulated thresholds shown in the right hand side of Fig. 6. The simulated thresholds for a chromaticity of zero and 0.05 lie both at around 3.45 mA and are higher than in the measurements by about 0.5 mA. At the same time, the simulated threshold for the slightly negative chromaticity matches the measurements at around 1 mA.

The measurements and the simulations were conducted for a range of positive and negative ADTS coefficients. No significant correlation between threshold currents and the value of the ADTS coefficient is observed in either measurement or simulations. This matches observations at other machines (e.g., [14]), while a potential dependence of the threshold on the tune spread has been reported in calculations [12,13], in cases where the tune spread is in the order of the synchrotron frequency. Despite the comparatively low synchrotron frequency at MAX IV (for an electron machine), this is not observed in the experiments at MAX IV.

This is not unexpected as the experimental ADTS coefficients reached only result in a very small tune shift for the center-of-mass oscillation and the bunch size observed in a stable beam. A typical measured ADTS coefficient of $b = 5000/\mathrm{m}$ leads with a stable bunch size of 10 μm or a center-of-mass movement with a maximal

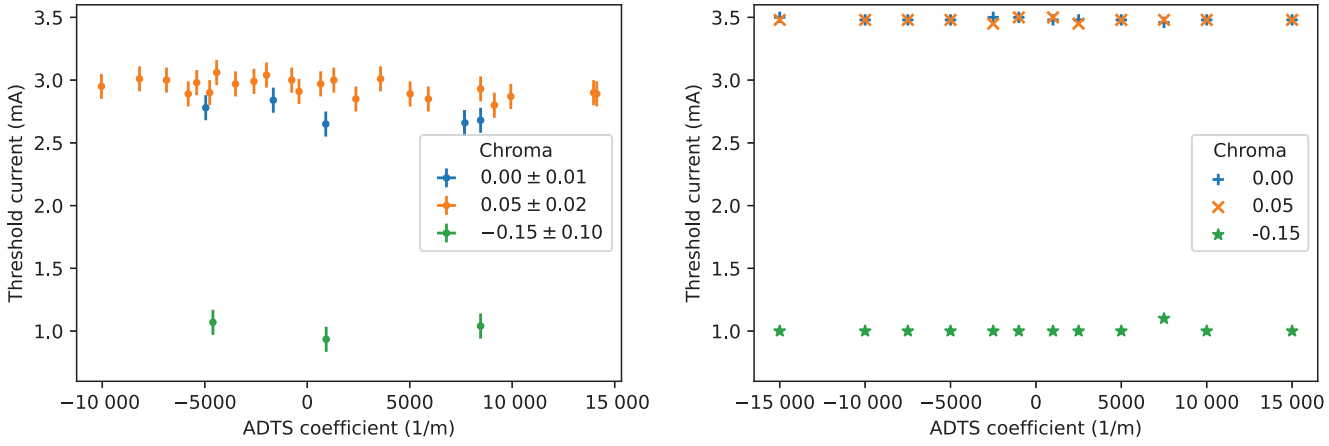


FIG. 6. Left: Single bunch threshold currents during injection shown as a function of ADTS coefficient measured at chromaticities of 0.00, 0.05, and −0.15. Right: Single bunch threshold currents simulated in MBTRACK2 (including bunch lengthening by addition longitudinal impedance) for chromaticities of 0.00, 0.05, −0.15.

amplitude of less than 10 μm (corresponding to an action of approximately $2 \times 10^{-11}$ m) to an estimated tune spread (see Appendix B) in the order of only $\approx 10^{-7}$. Consequently, an ADTS coefficient in this order of magnitude is not relevant until the instability starts to blow-up the beam leading to a bigger contribution of the ADTS due to the drastically increased center-of-mass oscillation and bunch size. As is shown in Fig. 3, during the instability, the center-of-mass amplitudes reach values of the order of hundreds of micrometers and, as will be shown later in Figs. 8 and 9, the bunch size blows up to similar sizes. Then the tune spread is in the order of ≈0.001, which corresponds already to two-thirds of the synchrotron tune. Therefore, it is there, above the instability threshold, that the ADTS is expected to influence the dynamics.

### B. Beam losses at threshold

A significant influence of the magnitude and sign of the ADTS coefficients can be observed in the amount of charge lost when the instability threshold is crossed during injection. Figure 7 shows the beam loss in percent for different values of the ADTS coefficient with a chromaticity close to zero or with slightly negative chromaticity values. For negative ADTS coefficients up to nearly zero ($\approx -500/\mathrm{m}$), no beam loss is encountered at all when crossing the instability threshold during injection. This is already noteworthy as it shows that the instability is not destructive even though it leads to strong center-of-mass oscillations and an increase in bunch size. On the other side, for positive ADTS coefficients, a partial beam loss is observed when crossing the threshold. For values from zero up to 6000/m, more than 40% and up to 90% of the beam current is lost. For higher positive ADTS coefficients, the loss goes down close to zero again. So, for ADTS coefficients up to 6000/m, there is a difference in the observed behavior for a positive and negative sign of the ADTS coefficient. While for negative coefficients the instability is self-containing, for positive coefficients a partial beam loss is observed until the remaining beam stabilizes again.

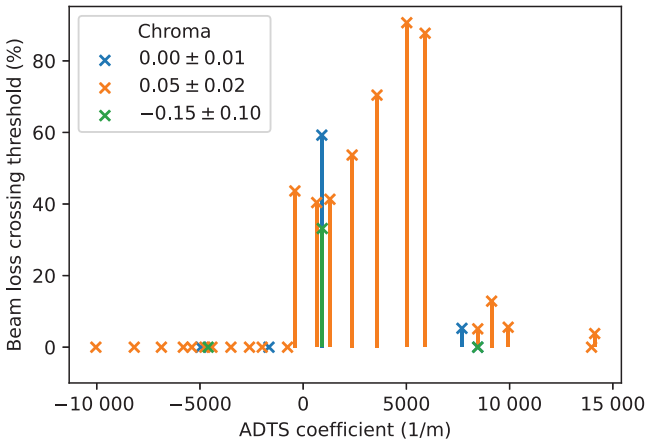


FIG. 7. Current loss in percent at the TMCI threshold as a function of the amplitude-dependent tune shift at chromaticities of 0, 0.05, and −0.15.

Similar asymmetries on the ADTS or the octupole magnet currents have been observed in the past in the damping of the transverse coherent motion associated with head-tail effects, for example, at SPEAR I [26] and at the KEK Photon Factory [27] and, as previously mentioned, this effect is well known and exploited at hadron machines [7–10]. This commonality suggests that Landau damping is also playing a role here, although the TMCI is considerably different to instabilities involving a single head-tail mode in isolation.

To investigate the observed differences in behavior above the threshold, the time domain signal of the center-of-mass oscillation and the bunch size was studied in measurement and simulation.

### C. Bunch position and size

For a negative ADTS coefficient, the dynamic above threshold shows clear, regular, sawtooth like bursts in transverse bunch size and as amplitude modulation of the center-of-mass oscillations. This is visible in the BPM trace directly (Fig. 3) as well as in the synchronous measurement of bunch position and bunch size in Fig. 8. The contribution of the bunch size can be seen in the difference in behavior over turns between the vertical beam size and center of mass. Additionally, the calculated spot size up to 0.68 mm (standard deviation determined by Gaussian fit) in Fig. 8 compared to the detected center-of-mass oscillation amplitude of maximal 0.4 mm (= 0.8 mm

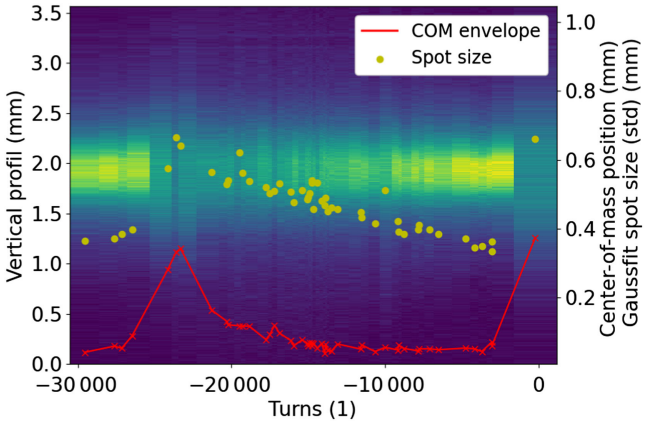


FIG. 8. Synchronized measurement of vertical spot profile and center-of-mass amplitude as a function of time. The image shows the vertical light spot measured at different points in the sawtooth like dynamic. In red, the envelope of the center-of-mass motion is displayed with a point for each spot profile measurement. The yellow dots indicate the spot size (std) gained from a Gaussian fit. Measured at ADTS coefficient $b = -10\,000/\mathrm{m}$ and current of 2.6 mA.

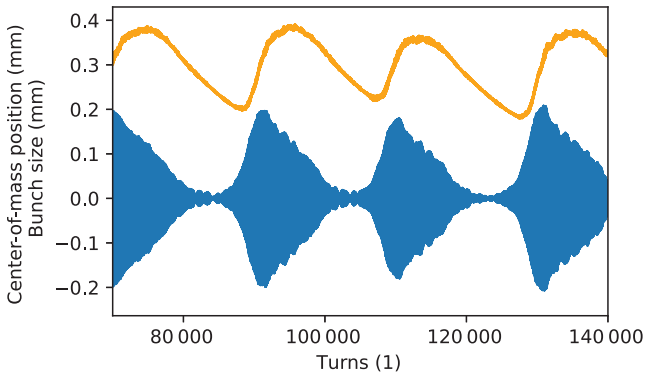


FIG. 9. Simulated center-of-mass oscillation and bunch size at an ADTS coefficient $b = -15\,000/\mathrm{m}$ and a current of 4.8 mA.

peak-peak) indicates that the bunch size has a non-negligible contribution. Furthermore, the center-of-mass oscillation goes back to nearly zero for some hundred turns between the increases in oscillation amplitude. During this time, the observed spot size slowly damps down indicating that the bunch size is damping down, reaching minimal values in the order of 0.35 mm before the next peak. The same sawtooth behavior is present in the simulation shown in Fig. 9 when synchrotron radiation effects, such as synchrotron radiation losses, synchrotron radiation damping, and quantum excitations, are included.

This dynamic indicates a stabilizing mechanism that leads to a containment of the instability instead of a continuous growth until charge is lost. The behavior in the amplitude of the center-of-mass oscillations and the bunch size show that at one point a temporary stabilization occurs which leads to a damping of the oscillation to below the noise limit of the measurement. The bunch size is also damped down during this stable period, but it does not reach the expected stable bunch size before the instability is triggered again leading to a fast blowup of the bunch size and the onset of strong center-of-mass oscillations. A possible mechanism behind these dynamics is Landau damping, which would also fit, as previously described, the observed asymmetry with respect to the ADTS sign.

The blown-up bunch size, increased COM oscillations, and the ADTS lead to an increased tune spread, which can cause a temporary increased Landau damping effect. The result can be described as a "self-containing" instability,[3] caused by Landau damping, which only sets when the bunch is blown-up and the ADTS results in a significant betatron tune spread. Two points can be identified in the dynamics. An "upper turning point" when the damping due to the ADTS caused by the blowup of the beam becomes predominant and overpowers the growth driven by the instability. A "lower turning point" when the bunch size and COM oscillations are damped down to such low values that the resulting tune spread (caused by the ADTS) is not enough to Landau damp the instability any longer and the growth starts again.

While the IBS is considered as the cause of the hysteresis observed in the instability threshold, it is not a candidate for explaining the self-containing dynamics, as it operates in the wrong sense, i.e., a blown-up beam has a lower threshold current and is, therefore, more unstable and does not contribute to a self-containing effect, where the threshold would need to increase to temporarily stabilize the unstable beam.

For positive ADTS, the dynamics above the threshold can only be observed in measurements at high ADTS coefficients where no instantaneous charge loss occurs. For higher bunch currents, the dynamics in the center-of-mass oscillation and the bunch size have a similar sawtooth like pattern as observed for negative ADTS coefficients (see left side of Fig. 10). The pattern changes for lower bunch currents, closer to the threshold, as shown in the right side in Fig. 10. Here, the center-of-mass oscillation amplitude is only lightly modulated in the measurements and nearly constant in the simulations.

The simulation results show that a positive ADTS (Fig. 10, lower left plot) leads to a stronger blowup than a negative ADTS (Fig. 9). The experiments (Figs. 3 and 10, upper left plot) show the same asymmetric behavior. This indicates that the level of blowup at which the instability is contained (the upper turning point in the center-of-mass motion) is different for negative and positive ADTS. The asymmetry is clearly visible in Fig. 11 where, for a bunch current slightly above threshold, the maximal bunch size and the maximal oscillation amplitude of the center-of-mass are given as a function of ADTS coefficient in simulations.[4] The range in ADTS coefficient where partial current loss occurs depends on the combination of the center-of-mass oscillations and the total bunch size which, above a certain value, leads to parts of the charge being "scraped" by the beam pipe. Independent of the exact value, it can be seen from Fig. 11 that the affected ADTS range would not be symmetric around zero but rather shifted to positive ADTS coefficients. The measurements show the same dependence of the maximal center-of-mass oscillation amplitude[5] as a function of the ADTS coefficient (Fig. 12) for negative ADTS. While it is not measurable at the lower positive ADTS coefficients, due to the partial beam losses, the measured values at higher positive ADTS coefficients are higher than the corresponding values at negative ADTS showing the same asymmetry as in the simulations in Fig. 11. From this follows, that to reach

[3]Similar behavior of a sawtooth-shaped instability contained by Landau damping has been seen, for example, at the APS for higher chromaticities [28].

[4]To be more robust against outliers the 95th percentile of the bunch size and the center-of-mass oscillation amplitude are taken.

[5]Again, the 95th percentile of center-of-mass oscillation is taken.

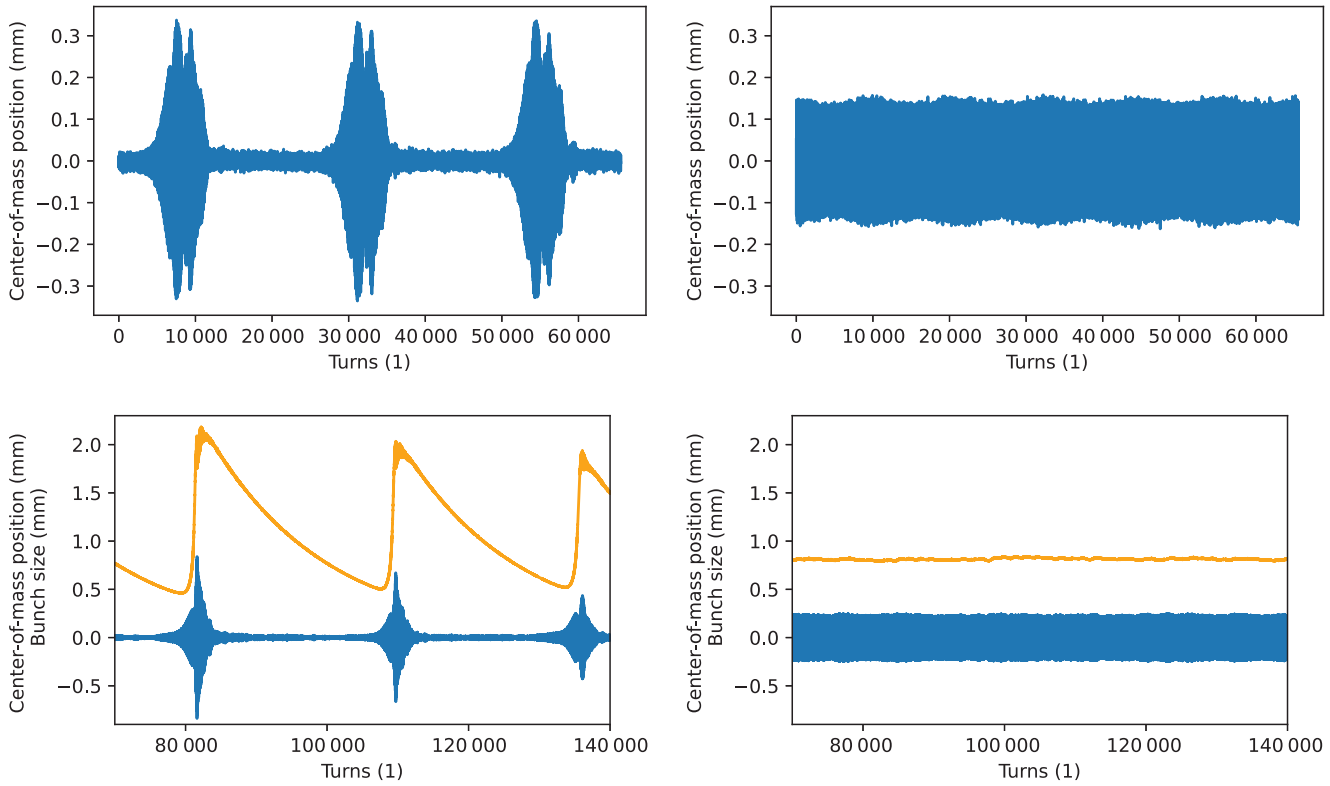


FIG. 10. Top: Measured center-of-mass oscillation at 3.07 mA (left) and 2.79 mA (right) and an ADTS coefficient $b = 13\,720/\mathrm{m}$. The measurement at high current shows a similar sawtooth pattern to measurements at negative ADTS coefficient (Fig. 3). The measurement at low current is more constant (noise level would be $\pm 0.02$ mm). Bottom: Simulated center-of-mass oscillation and bunch size at $b = 15\,000/\mathrm{m}$ and bunch currents of 4.8 mA (left) and 4.6 mA (right).

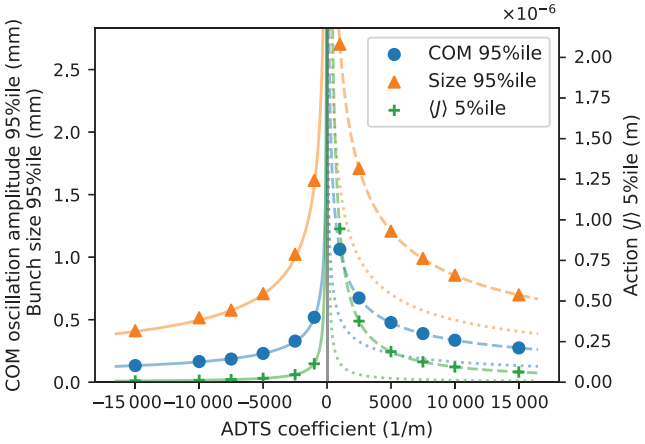


FIG. 11. Simulated maximal (95th percentile) bunch size and center-of-mass oscillation amplitude and minimal (5th percentile) action $\langle J \rangle$ as a function of the ADTS coefficient for currents slightly above threshold. The lines highlight the $1/x^{1/2}$ (bunch size and COM) respective $1/x$ ($\langle J \rangle$) dependency with the dotted line being the mirror of the solid line at negative ADTS.

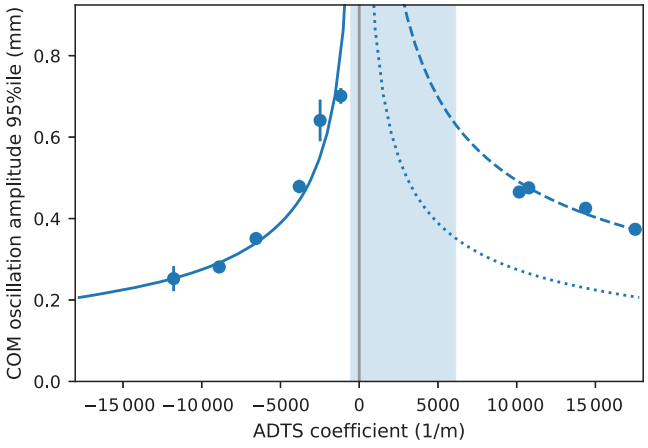


FIG. 12. Measurements of the maximal center-of-mass oscillation amplitude (95th percentile) as a function of the ADTS coefficient. The measurements were taken at bunch currents close to the threshold and with a chromaticity of 0.05. The lines highlight the $1/x^{1/2}$ dependency with the dotted line being the mirror of the solid line at negative ADTS. The errors show the standard deviation between multiple consecutive measurements per point.

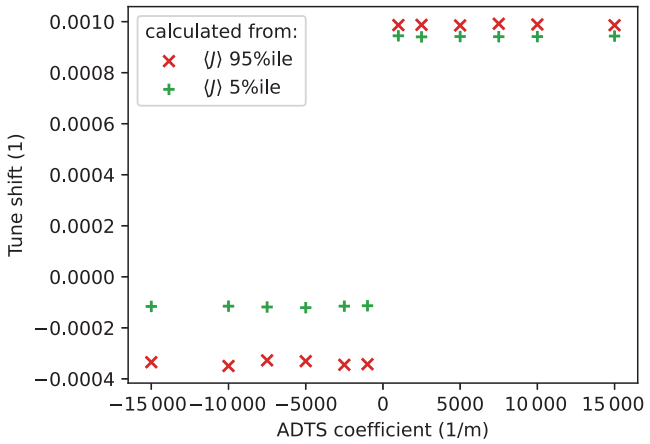


FIG. 13. Tune shift calculated from the maximal (95th percentile) and the minimal (5th percentile) action $\langle J \rangle$ as a function of ADTS coefficient.

the same level of suppression of the instability (meaning low values in maximal bunch size and center-of-mass oscillations), a higher absolute value for a positive ADTS coefficient is needed than for a negative ADTS coefficient. This asymmetry in the measured and simulated beam sizes provides an explanation for the asymmetry observed in the proportion of the current lost when crossing the instability threshold (see Fig. 7).

Figure 11 also shows the value of the average action of the particle ensemble $\langle J \rangle$ at the times of minimal bunch size and center-of-mass oscillations[6] as a function of ADTS coefficient, again the asymmetry for the different signs of the ADTS coefficient is visible. The minimal value $\langle J \rangle$ reaches can be connected to the point were the instability is no longer damped and the beam becomes unstable again, the lower turning point of the dynamics.

Both the maximal bunch size and center-of-mass oscillation amplitudes as well as the minimal action $\langle J \rangle$ show the characteristic dependence on the ADTS coefficient. For $\langle J \rangle$, it follows a $1/x$ dependency and the bunch size as well as the center-of-mass oscillation amplitude has a $1/\sqrt{x}$ dependency. This again indicates the connection with the amplitude-dependent tune shift, via Eq. (3).

Under the assumptions of, first, a Gaussian distribution[7] and, second, no center-of-mass movement, the tune shift at $\langle J \rangle$ is equal to the tune spread in the bunch (see Appendix B). These assumptions are most justified at the "lower turning point" where the COM motion is negligible. For the rest of the sawtooth period, due to the linear nature of the ADTS (as a function of $J$), it can be assumed that a center-of-mass movement only increases the actual tune spread. Figure 13 shows the results of applying this approximation to the average particle actions displayed in Fig. 11. In Fig. 13, it is visible that the calculated tune shift (and approximate spread) at the fifth percentile in average particle action $\langle J \rangle$ (the lower turning point) for each ADTS coefficient shows a constant but different levels of tune shift for each sign of the ADTS. While for negative ADTS the calculated tune shift of ≈0.00012 is approximately 8% of the synchrotron tune, the shift for positive ADTS is with ≈0.00094 already 65% of the synchrotron tune. This significant difference implies that for positive and negative ADTS, a different level of tune spread is required to contain the instability via sufficient Landau damping. The tune shift calculated from the 95th percentile $\langle J \rangle$ (the upper turning point) shows a very similar behavior, where the small difference between maximal and minimal values on the positive side of the ADTS is explained by the fact that nearly no sawtooth is observed for positive ADTS coefficients and currents close to the threshold (compare Fig. 10). We conclude that the tune shift stays between these two levels, with the higher one being the point were the beam stabilizes and starts to damp (upper turning point) and the lower one indicates when the stabilizing effect stops and the beam goes unstable and blows up again (lower turning point). And while the overall behavior is the same for both signs of the ADTS, the tune shift at the turning points is significantly higher for positive ADTS coefficients.

That this behavior can be attributed to Landau damping is further supported in the following section by theoretical calculations comparing the instability growth rates of the transverse mode coupling against Landau contours.

### D. Theoretical calculations

The theory for Landau damping in combination with transverse mode coupling by Chin (see Sec. I A) is valid for a system with no coherent perturbations, which, in the observed dynamics above the instability threshold, is only approximately reached at the "lower turning point" where no significant center-of-mass motion occurs. For the following discussion, we nevertheless use Chin's equations to interpret qualitatively the results of experiment and tracking.

Figure 14 shows stability diagrams calculated from Eq. (4) for the cases of positive and negative ADTS. Contours (for a very slightly positive growth rate) are drawn by plotting the imaginary part of the inverse dispersion relation $I_m^{-1}$ against the real part. These contours map out the expected asymmetric shape in complex frequency space pointing toward negative coherent tune shifts in the case of negative ADTS. Changing the sign of the ADTS to positive reflects the contour about the line of zero coherent frequency shift. Also shown in this figure are the eigenvalues of the coupling matrix in Eq. (6) without Landau damping where two modes are included: the azimuthal head-tail modes $m = 0$ and $m = -1$. As radial modes have been neglected in order to make the image

[6]The 5th percentile is taken as value for the minimal action $\langle J \rangle$.
[7]Effects of Gaussian distributions with cut tails have been discussed in [9,29].

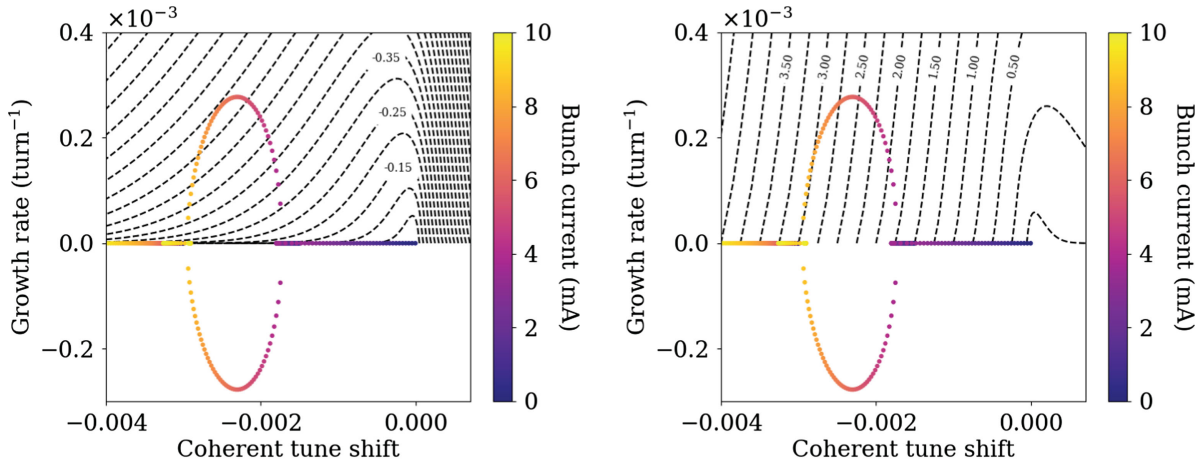


(a) Negative ADTS

(b) Positive ADTS

FIG. 14. Stability diagrams for negative ADTS coefficient (a) and positive ADTS coefficient (b). The numbers that label the Landau contours indicate the magnitude of the tune spread quantified by $\sigma_\nu = \Delta\nu(\langle J \rangle)$ scaled with $10^3$ for readability, equivalent to the product $b \cdot \langle J \rangle$ [see Eq. (3)]. The colored points are the eigenvalues of the scaled coupling matrix $\nu_s \mathbf{M}_{nl}^{mk}$ where the color represents the bunch current.

clearer, it can be observed (contrary to measurements) that the beam becomes stable again at higher currents. The calculations were performed with an internal code [30], which was bench marked against DELPHI [31] (see Appendix A).

For a head-tail mode to be stable in isolation, its complex coherent frequency shift would have to be within the Landau contour.[8] The condition in the presence of mode coupling is slightly different and given by the zero determinant in Eq. (6). How these diagrams are best applied to the TMCI to solve Eq. (6) is an active research topic, discussed for example in [2,32]. Nonetheless, the images in Fig. 14, derived by evaluating the inverse dispersion relation $I_m^{-1}$ and the coupling matrix $\mathbf{M}$ individually, are still illustrative. It can be seen that, in order to influence the stability, a positive ADTS coefficient must be much larger in magnitude than a negative one, matching the observations in measurement and simulation shown in Figs. 11 and 12. This is intuitive as a negative ADTS coefficient means that the tune spread is toward negative tune shifts and the current-dependent tune shift of the $m = 0$ mode is also negative for most broadband impedances. Therefore, the shifted coherent tune frequency lies within the band of the incoherent tune and motions with this tune frequency are damped by the Landau damping effect. Furthermore, it can be seen that for a stable beam with a small value $\langle J \rangle$ combined with a typical ADTS value $b = 5000/\mathrm{m}$ (as discussed in Sec. IV A), the stability contours ($\Delta\nu \approx 10^{-7}$) are so small that they do not cover the tune shift at the threshold current. Therefore, the Landau damping does not affect the beam directly at the threshold that agrees with the experimental observations.

As stated, Chin's model ignores the complexities associated with the large amplitude oscillations that are present when the beam is unstable. Nevertheless, it successfully predicts the qualitative results of the experimental investigation presented in Secs. IV B and IV C. We can, therefore, conclude that the Landau contours are similarly skewed also in the case of an unstable beam.

One feature of storage rings used for fourth-generation synchrotron light sources, particularly those using low-rf frequencies (such as the 100 MHz of the 3 GeV ring at MAX IV), which is beneficial in the context of Landau damping, the TMCI instability is the low incoherent synchrotron frequency. This means that the coupling frequency of the $m = 0$ and $m = -1$ head-tail modes is not so far out of the spread in betatron tune of the electron bunches. Nevertheless, as mentioned in Sec. IV A, for MAX IV an increase in the beam size (and thereby the tune spread) is required for Landau damping to kick in.

### E. Betatron tune shift with current

Observing the vertical betatron tune as a function of current directly shows the expected current-dependent tune shift due to the transverse impedance from the zero-current tune of $\nu_0 = 0.275$ toward the $-1$ mode at the first synchrotron frequency side band ($\nu_0 - 0.00146$). In simulations of the coherent beam spectrum, the threshold of the TMCI is clearly visible as the current at which the tune couples to the $-1$ mode (top row in Fig. 15). This is the same for both signs of the ADTS. The difference for negative and positive ADTS starts above the threshold

[8]The form of the contours are independent of the mode number $m$ because, as can be seen by inspection of Eq. (5), a change of $m$ simply results in a shift of position along the contour.

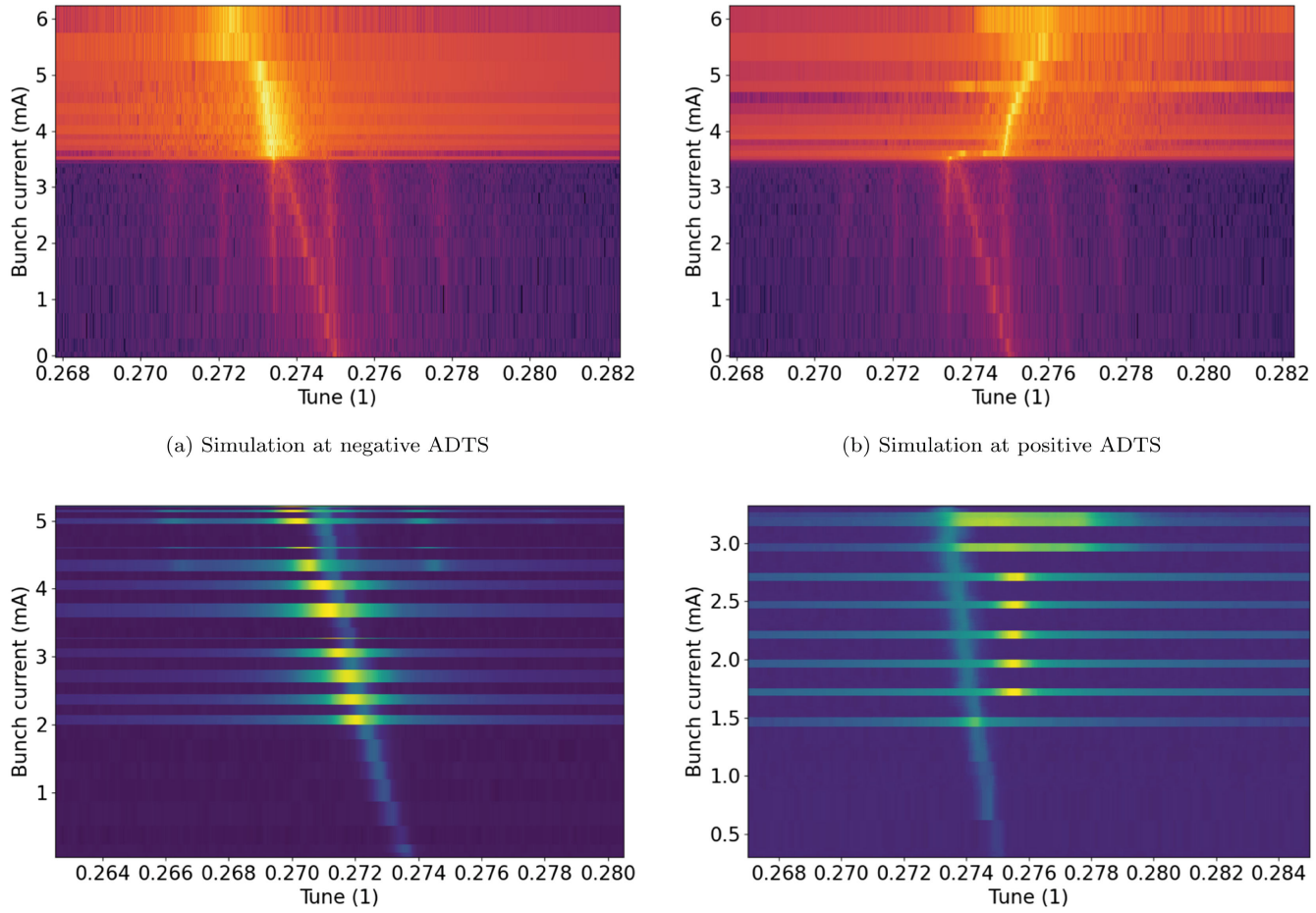


(a) Simulation at negative ADTS

(b) Simulation at positive ADTS

(c) Measurement at negative ADTS

(d) Measurement at positive ADTS

FIG. 15. Coherent motion spectrum showing the current-dependent betatron tune shift below and above the instability threshold. Simulation (a, b): Fourier transform of the center-of-mass oscillation plotted as a function of the bunch current for negative (a) and positive (b) ADTS coefficient $b = 15\,000/\mathrm{m}$. Measurement (c, d): Fourier transform of the center-of-mass oscillation as a function of bunch current for an ADTS coefficient of $b = -10\,000/\mathrm{m}$ (c) and $b = 13\,720/\mathrm{m}$ (d). During the measurement, the instability was "switched" on and off.

current, where for negative ADTS the tune continues its shift toward a lower tune with a similar slope as below the threshold [Fig. 15(a)]. For the positive ADTS, the behavior looks very different. While a slight shift in the opposite direction to higher tunes would not be unexpected, due to the positive sign of the ADTS, the tune jumps within a very small current range above the threshold from the $-1$ mode back to the 0 mode and then shows a continuous shift to higher tunes from there [Fig. 15(b)].

This drastic difference in behavior can also be seen in measurements. Figures 15(c) and 15(d) show the measured tune spectra at different bunch currents and for negative and positive ADTS, respectively. The measurements were conducted in such a way that the previously described hysteresis of the instability threshold (Sec. IV A) was used to get comparative measurements for the tune of a stable and an unstable beam. To this end, the measurement was started at high bunch currents and the tune spectrum was recorded alternately for a beam stabilized by the BBB feedback system[9] and for an unstable beam, where the instability was triggered by a short excitation.[10]

For the stable beam, the tune continues its current-dependent shift toward lower values. For both signs of the ADTS, it is clearly visible that the presence of the instability shifts the tune compared to the tune of the stable beam. For negative ADTS [Fig. 15(c)], the shift is small and toward slightly lower tune values. For positive ADTS [Fig. 15(d)], the tune is shifted back toward the zero-current tune (0 mode) and shows a very small current-dependent shift toward higher tune. Except for the difference in threshold and the threshold hysteresis observed in the measurements, the simulation and the measurements agree

[9]After initial stabilization, the feedback is switched off during the measurement.

[10]The excitation is switched off as well before the measurement is taken.

qualitatively very well with respect to the tune shifts below and above threshold.

At higher bunch currents, additional features appear. In the measurement at negative ADTS, an upper and lower sideband shows up, moving with the tune as a function of current. In the case of the positive ADTS, the tune peak is broadened greatly and nearly spans from the $-1$ mode to the $+1$ mode. Comparing with the calculated tune shift of $\approx 0.001$ resulting from the maximal action $J$ simulated in case of positive ADTS (Fig. 13) shows that the jump of the coherent betatron tune by one synchrotron tune ($\nu_s = 0.00146$) toward the 0 mode is only slightly bigger. Overall, from the measurement and tracking simulations, it is not apparent whether this difference in the behavior of the coherent tune above threshold is the cause or a consequence of the observed asymmetry in the level of beam blowup for negative versus positive ADTS.

## V. SUMMARY AND CONCLUSION

In this paper, we showed experimentally how the amplitude-dependent tune shift and the resulting Landau damping affects the dynamics of the transverse mode-coupling instability under certain operational parameters at a fourth-generation synchrotron light source. While during routine operations, the bunch current at the 3 GeV ring at the MAX IV Laboratory is below the TMCI threshold, an asymmetric dependence on the sign of the ADTS has been previously observed in dedicated experiments. Systematic studies were now conducted to investigate this observed asymmetry in dedicated a single bunch experiments. It was observed that for some ADTS coefficients the beam was lost when crossing the threshold while at others a saw-tooth shaped amplitude modulation occurs on the center-of-mass oscillation as well as on the bunch size leading to a self-contained instability. While this paper focuses on the vertical plane, preliminary experiments in the horizontal plane have shown a similar asymmetry with respect to the sign of the ADTS coefficient.

The presented measurements and the simulations with the tracking tool MBTRACK2 are in good agreement. Both show that the observed threshold current is independent of the ADTS coefficient and an observed hysteresis in the measured threshold can be attributed to intrabeam scattering effects. For the dynamics above the threshold, both measurement and simulation show that for positive ADTS coefficients, the maximal center-of-mass oscillation amplitude and bunch size, that is reached before the instability stabilizes, is systematically higher than for negative ADTS coefficients, indicating that this could be the cause of the observed partial beam current losses. The same asymmetry is also visible in the tune spread at the minimal $\langle J \rangle$ required for damping. The spread is constant and the value is only dependent on the sign of the ADTS, with the tune spread calculated for positive ADTS coefficients already being at $\approx 65\%$ of the synchrotron tune. Stability diagrams with Landau contours calculated to include the amplitude-dependent tune shift show as well that higher positive ADTS coefficients compared to negative ones are required for the instability to be Landau damped. Furthermore, simulations and measurements of the coherent tunes as a function of the bunch current show a strong difference in the tunes development above threshold. For negative ADTS coefficients, the tune is slightly shifting to lower values starting from the $-1$ mode at the threshold. In contrast, for positive ADTS coefficients, the coherent tune jumps back to the 0 mode and only then shows with increasing current a slight shift to higher tune values, as might be expected for positive ADTS coefficients.

Our experiments and analysis show an asymmetry in how strongly the vertical TMCI is self-containing and of which tune shift with current is observed above the threshold. As expected, a higher absolute value of the ADTS coefficient leads to a lower maximal center-of-mass oscillation and bunch size blowup. But when comparing signs, a higher positive ADTS coefficient is required for the same amount of suppression of the instability than for a negative ADTS. The intuitive explanation behind this is that the ADTS contributes asymmetrically to the Landau damping depending on the ADTS sign, as the resulting tune spread either covers the same lower frequencies as the tune shift with current by impedance or it goes in the other direction toward higher frequencies reducing the resulting Landau damping effect significantly as seen in the presented results for positive ADTS coefficients.

In conclusion, it can be said that while the asymmetric dependence of the Landau damping on the ADTS sign is known in connection with several transverse instabilities, mainly at hadron machines, the effect on the TMCI had not been investigated in such detail before. In the presented investigation at the MAX IV 3 GeV ring, the instability threshold of the TMCI was, as observed previously [14], unaffected by the ADTS. However, the Landau damping induced by the amplitude-dependent tune shift significantly affects the dynamics above threshold. Depending on the amplitude and sign of the ADTS, the beam is not lost, as observed in most synchrotron light sources but experiences a self-contained instability. It could be shown in the measurement as well as in tracking simulations and theoretical stability considerations that the maximal level reached by the center-of-mass motion and bunch size before being contained is lower for a negative than for a positive sign of the ADTS coefficient, pointing back to Landau damping as reason for these dynamics.

We suspect that the observation of this behavior is caused by, among other parameters, the rather low synchrotron frequency at MAX IV. It might be one of the contributions for Landau damping and the resulting asymmetry to become relevant and in making it observable. The low momentum compaction factor, typical for fourth-generation light-source storage rings, is combined with the low rf frequency of 100 MHz. Both of these aspects lead to

a synchrotron frequency that then lies within the betatron tune spread of the bunch when it is blown up by the instability. This, therefore, puts the betatron tune at the point of mode coupling within the reach of the Landau damping before the beam hits the vacuum chamber wall and is lost. The role of the low synchrotron frequency in enabling these dynamics indicates that the presented findings will become more relevant in the future fourth-generation light-source storage rings with even more extreme parameters than MAX IV.

## ACKNOWLEDGMENTS

We thank the operations team at MAX IV for their support during experiments. The computations were enabled by resources provided by LUNARC.

## APPENDIX A: BENCHMARKING OF INTERNAL CODE AGAINST DELPHI

This section describes a partial benchmarking of the code [30] developed at MAX IV used to generate Fig. 14 against the existing DELPHI code. There are two parts to this: the first is the calculation of the Landau contours. This is benchmarked for a tune spread, corresponding to a tune shift at the average action, $\sigma_\nu = \Delta\nu(\langle J\rangle) = b\langle J\rangle = 0.28\times10^{-3}$ and the machine parameters in Table I. The comparison between the two codes is shown in Fig. 16.

The second part is benchmarking of the coherent tune shifts and growth rates with the beam current in the absence of Landau damping. These calculations were carried out for the same parameters and the impedance model introduced in Sec. III. For completeness, more radial and azimuthal modes were included than in Fig. 14 but the agreement is maintained for the lower number of modes. The results are shown in Fig. 17. These figures show that the two codes, independently developed, produce the same results and so we can proceed using the in-house code with confidence.

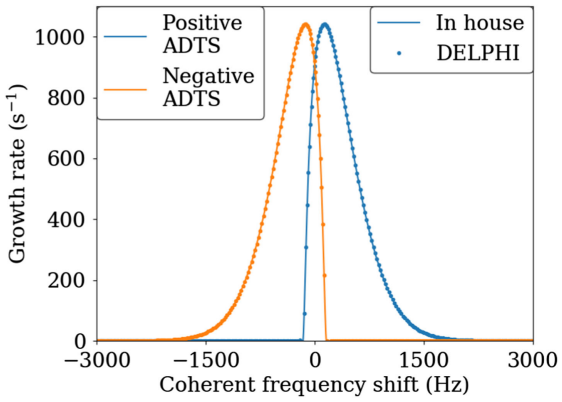


FIG. 16. Landau contours at the transition between negative and positive growth rate as generated using DELPHI (dots) and the code developed in house (lines) for positive (blue) and negative (orange) sign of the ADTS.

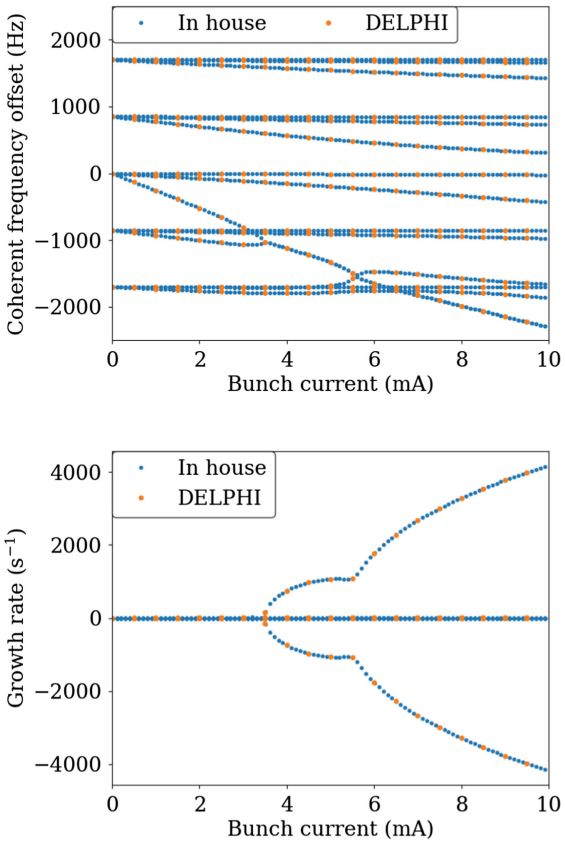


FIG. 17. Coherent frequency shifts (top) and growth rates (bottom) as a function of the beam current as calculated using DELPHI (orange) and the code developed in house (blue).

## APPENDIX B: TUNE SHIFT AND SPREAD FOR A GAUSSIAN CHARGE DISTRIBUTION

This section gives a simple derivation for the tune spread $\sigma_\nu$ introduced by the amplitude-dependent tune shift in a simple Gaussian charge distribution with a center-of-mass position of 0.

In the main part of the paper, Eq. (3) is used to linearly relate the shift in tune due to the ADTS with the action $J$ of a particle. The charge distribution is given by the simple Gaussian in Eq. (2). From this, the average betatron tune $\bar{\nu}$ and the rms tune spread $\sigma_\nu$ can be calculated as follows:

$$\begin{aligned}
\bar{\nu} &= \int_0^\infty \int_0^{2\pi} \nu(J) f(J) dJ d\psi, \\
\bar{\nu} &= \int_0^\infty \int_0^{2\pi} [\nu(0) + bJ] \frac{1}{2\pi\langle J\rangle} e^{-\frac{J}{\langle J\rangle}} dJ d\psi, \\
\bar{\nu} &= \nu(0) + b\langle J\rangle, \\
\sigma_\nu^2 &= \int_0^\infty \int_0^{2\pi} (\nu(J) - \bar{\nu})^2 f(J) dJ d\psi, \\
\sigma_\nu^2 &= \int_0^\infty \int_0^{2\pi} (b^2J^2 + b^2\langle J\rangle^2 - 2b^2 J\langle J\rangle) f(J) dJ d\psi, \\
\sigma_\nu^2 &= b^2\langle J\rangle^2.
\end{aligned} \tag{B1}$$

This shows that for a simple Gaussian charge distribution centered around zero, the tune spread $\sigma_\nu$ caused by the ADTS is equal to the tune shift a particle at the position of $\langle J \rangle$ has

$$\sigma_\nu = b\langle J \rangle = \Delta\nu(\langle J \rangle). \tag{B2}$$

The complexity increases significantly for a nonzero center-of-mass position of the charge distribution. Given the linear form of the ADTS as a function of $J$, a nonzero center-of-mass position leads to an increased tune spread compared to the case with a zero center-of-mass position of the Gaussian distribution.


[1] H. G. Hereward, Landau damping by non-linearity, CERN, Geneva, Technical Report No. CERN-MPS-DL-69-11, 1969, https://cds.cern.ch/record/1114390.

[2] N. Mounet, Landau damping in the transverse plane, CERN Yellow Reports: Conference Proceedings (2020), Vol. 9, 10.23732/CYRCP-2020-009.45.

[3] L. Carver, X. Buffat, K. Li, E. Metral, and M. Schenk, Transverse beam instabilities in the presence of linear coupling in the Large Hadron Collider, Phys. Rev. Accel. Beams **21**, 044401 (2018).

[4] G. Skripka, A. Andersson, F. Cullinan, R. Nagaoka, and P. Tavares, Impedance characterization and collective effects in the MAX IV 3 GeV ring, in *Proceedings of the Third North American Particle Accelerator Conference, NAPAC-2016, Chicago, IL* (JACoW, Geneva, Switzerland, 2017), pp. 843–846, 10.18429/JACoW-NAPAC2016-WEA3CO04.

[5] P. F. Tavares, E. Al-Dmour, Å. Andersson, F. Cullinan, B. N. Jensen, D. Olsson, D. K. Olsson, M. Sjöström, H. Tarawneh, S. Thorin, and A. Vorozhtsov, Commissioning and first-year operational results of the MAXIV 3 GeV ring, J. Synchrotron Radiat. **25**, 1291 (2018).

[6] F. J. Cullinan, Collective effects in MAX IV, in *Proceedings of the 7th Low Emittance Rings Workshop* (2018), https://indico.cern.ch/event/671745/contributions/2794231/.

[7] X. Buffat, W. Herr, N. Mounet, T. Pieloni, and S. White, Stability diagrams of colliding beams in the large hadron collider, Phys. Rev. ST Accel. Beams **17**, 111002 (2014).

[8] X. Buffat, S. Antipov, G. Arduini, R. De Maria, N. Karastathis, S. Kostoglou, A. Koval, E. H. Maclean, N. Mounet, Y. Papaphilippou, T. H. B. Persson, and R. Tomas Garcia, Strategy for Landau damping of head-tail instabilities at top energy in the HL-LHC (2020), https://cds.cern.ch/record/2745703.

[9] E. Métral, General mitigation techniques for coherent beam instabilities in particle accelerators, Eur. Phys. J. Plus **137**, 47 (2022).

[10] C. Tambasco, S. Arsenyev, J. B. García, X. Buffat, T. Pieloni, L. Rivkin, and D. Schulte, Landau damping studies for the FCC: Octupole magnets, electron lens and beam-beam effects, in *Proceedings of the 9th International Particle Accelerator Conference, IPAC-2018, Vancouver, BC, Canada* (JACoW, Geneva, Switzerland, 2018), pp. 3150–3153, 10.18429/JACoW-IPAC2018-THPAF074.

[11] L. Tosi, V. Smaluk, and E. Karantzoulis, Landau damping via the harmonic sextupole, Phys. Rev. ST Accel. Beams **6**, 054401 (2003).

[12] E. Métral, Landau damping for TMCI: With versus without transverse damper, CERN, Geneva, Technical Report No. CERN-ACC-NOTE-2019-0018, 2019, http://cds.cern.ch/record/2674776.

[13] Y. H. Chin, Hamiltonian formulation for transverse bunched beam instabilities in the presence of betatron tune spread, CERN, Geneva, Report No. CERN SPS/85-9, 1985, https://cds.cern.ch/record/160217/files/198507010.pdf.

[14] R. R. Lindberg, Fokker-planck analysis of transverse collective instabilities in electron storage rings, Phys. Rev. Accel. Beams **19**, 124402 (2016).

[15] A. Gamelin, W. Foosang, and R. Nagaoka, MBTRACK2, a Collective Effect Library in Python, in *Proceedings of the 12th International Particle Accelerator Conference, IPAC-2021, Campinas, Brazil* (JACoW, Geneva, Switzerland, 2021), pp. 282–285, 10.18429/JACoW-IPAC2021-MOPAB070.

[16] P. F. Tavares, S. C. Leemann, M. Sjöström, and Å. Andersson, The MAXIV storage ring project, J. Synchrotron Radiat. **21**, 862 (2014).

[17] S. Kostoglou, N. Karastathis, Y. Papaphilippou, D. Pellegrini, and P. Zisopoulos, Development of computational tools for noise studies in the LHC, in *Proceedings of the International Particle Accelerator Conference, IPAC-2017, Copenhagen, Denmark* (JACoW, Geneva, Switzerland, 2017), 10.18429/JACoW-IPAC2017-THPAB044.

[18] K. Paraschou and S. Kostoglou, and D. Pellegrini, Nafflib, https://github.com/PyCOMPLETE/NAFFlib.

[19] J. Breunlin and A. Andersson, Emittance diagnostics at the Max Iv 3 Gev storage ring, in *Proceedings of the 7th International Particle Accelerator Conference, IPAC-2016, Busan, Korea* (JACoW, Geneva, Switzerland, 2016), pp. 2908–2910, 10.18429/JACoW-IPAC2016-WEPOW034.

[20] MBTRACK2, tag 0.4, https://gitlab.synchrotron-soleil.fr/PA/collective-effects/mbtrack2/-/tree/0.4?ref_type=tags.

[21] See Supplemental Material at http://link.aps.org/supplemental/10.1103/PhysRevAccelBeams.27.104402 for a python script that can be used to start the presented MBTRACK2 simulations. It contains the information on the used parameters and furthermore shows which MBTRACK2 functions were used to include, e.g., impedances or beam dynamics. It also contains a small extension to the MBTRACK2 synchrotron class that allows to save the properties of the synchrotron class object together with the simulation results in the output hdf5 file, created with support by P. Schreiber, SOLEIL.

[22] G. Skripka, R. Nagaoka, M. Klein, F. Cullinan, and P. F. Tavares, Simultaneous computation of intrabunch and interbunch collective beam motions in storage rings, Nucl. Instrum. Methods Phys. Res., Sect. A **806**, 221 (2016).

[23] A. W. Chao, *Physics of Collective Beam Instabilities in High-Energy Accelerators* (Wiley, New York, 1993), ISBN 978-0-471-55184-3.

[24] P. Alexandre, R. B. E. Fekih, A. Letrésor, S. Thoraud, J. da Silva Castro, F. Bouvet, J. Breunlin, Åke Andersson,

and P. Fernandes Tavares, Transparent top-up injection into a fourth-generation storage ring, Nucl. Instrum. Methods Phys. Res., Sect. A **986**, 164739 (2021).

[25] K. Y. Ng, *Physics of Intensity Dependent Beam Instabilities* (World Scientific, Hoboken, NJ, 2006), p. 776.

[26] The SPEAR Group, Fast damping of transverse coherent dipole oscillations in SPEAR, in *Proceedings of the 9th International Conference on High-Energy Accelerators* (1974), pp. 338–340, https://www.osti.gov/servlets/purl/1443110.

[27] K. Ohmi and Y. Kobayashi, Head-tail effect due to lattice nonlinearities in storage rings, Phys. Rev. E **59**, 1167 (1999).

[28] K. C. Harkay, Z. Huang, E. Lessner, and B. X. Yang, Transverse sawtooth instability at the advanced photon source, in *Proceedings of the 19th IEEE Particle Accelerator Conference, Chicago, IL* (IEEE, New York, 2001), https://cds.cern.ch/record/556224.

[29] E. Métral and A. Verdier, Stability diagram for Landau damping with a beam collimated at an arbitrary number of sigmas, CERN, Geneva, Technical Report No. CERN-AB-2004-019-ABP, 2004, https://cds.cern.ch/record/733611.

[30] https://github.com/fracul/adts-maxiv

[31] N. Mounet, D. Amorim, and N. Biancacci, Delphi, https://gitlab.com/IRIS_mirror/DELPHI_mirror.

[32] E. Métral, Imaginary tune split and repulsion single-bunch instability mechanism in the presence of a resistive transverse damper and its mitigation, Phys. Rev. Accel. Beams **24**, 041003 (2021).